

Automated Relocation of the Petermann Ranges Aftershock Sequence

Gregory Brenn¹, Sharmin Shamsalsadati¹, Christian Sippl², and Mustafa Comoglu¹

1. Geoscience Australia, Symonston, ACT. Email: Gregory.Brenn@ga.gov.au

2. Czech Academy of Sciences, Prague, Czech Republic

Abstract

The Mw 6.1 Petermann Ranges earthquake that occurred on 20 May, 2016 in the Central Ranges, NT, is the largest onshore earthquake to be recorded in Australia since the 1988 Tennant Creek sequence. While geodetic and geophysical analyses have characterised the extent of surface rupture and faulting mechanism respectively, a comprehensive aftershock characterization has yet to be performed. Data has been acquired from a 13-station temporary seismic network deployed jointly by the ANU and Geoscience Australia (GA), collected from five days following the mainshock to early October. Taking advantage of enhanced automatic detection techniques using the SeisComP3 earthquake monitoring software within the National Earthquake Alerts Centre (NEAC) at GA, we have developed a comprehensive earthquake catalogue for this mainshock-aftershock sequence. Utilising the NonLinLoc location algorithm combined with a Tennant Creek-derived velocity model, we have preliminarily located over 5,200 aftershocks. With additional spatio-temporal analyses and event relocation, our objective will be to use these aftershocks to help delineate the geometry of the headwall rupture along the Woodroffe Thrust. These high-resolution aftershock detection techniques are intended to be implemented in real-time within the NEAC following future significant Australian intraplate earthquakes.

Keywords: Earthquake catalogue, Petermann Ranges, Aftershock Analysis, SeisComP



© Commonwealth of Australia (Geoscience Australia) 2021
<http://www.creativecommons.org/licenses/by/4.0/legalcode>

1 Introduction

Surface-rupturing earthquakes in Stable Continental Regions (SCR) such as in Australia occur infrequently, which inherently leads to challenges when characterizing these seismic sources and their associated seismic hazard (Allen, 2019). Australia on average experiences two earthquakes of $M \geq 5$ per year, which is a relatively high rate of seismicity for a SCR, and Geoscience Australia has recorded over 11,000 earthquakes since 2000, not including the events detected in this study (Johnston, 1994b; www.earthquakes.ga.gov.au; last accessed Oct 2021). These larger intraplate earthquakes in Australia are suggested to be associated with continued deformation within the Australian Plate, in response to distal plate boundary forces (Clark et al., 2012). Following significant earthquakes, rapid development of a high-resolution seismic catalogue of aftershocks can provide essential information to guide earthquake response, can help to reveal previously unidentified faults, and can provide new insights into the understanding of the seismic hazard of intraplate faults and the seismotectonics controlling their rupture process (e.g., Shelly, 2020; Waldhauser, 2004).

The National Earthquake Alerts Centre (NEAC) at Geoscience Australia recently upgraded its earthquake monitoring capabilities by implementing the SeisComP seismological software package into their real-time data acquisition, processing, and analysis activities (Weber et al., 2007). SeisComP is a powerful tool that provides advanced resources for both dissemination of earthquake products and data processing techniques, which among other priorities, greatly advances Geoscience Australia's capabilities to rapidly characterise aftershock sequences in semi real-time.

On 20 May 2016 at approximately 18:14 UTC, a Mwp 6.1 earthquake was recorded in the Petermann Ranges of the Northern Territory (NT) and was the largest onshore earthquake to have been recorded in Australia since the 1988 Tennant Creek earthquake (Jones et al., 1991; www.earthquakes.ga.gov.au; last accessed Oct 2021). The epicentre for this event was located approximately 460 km southwest of Alice Springs and approximately 125 km west of Uluru, in a remote and sparsely inhabited area of southwest Northern Territory (Figure 1). Fortunately, no significant damage or loss of life was reported.

Seismic source inversion modelling results indicate a shallow rupture depth of approximately 1 km (Hejrani and Tkalčić, 2019), and the USGS W-phase solution estimated a depth of 10 km. Multiple interferometric synthetic aperture radar (InSAR) models suggest the earthquake ruptured along a northeast-dipping plane at an angle of 22-39° (Polcari et al., 2018; Wang et al., 2019), with coseismic slip models suggesting dominant thrust motion with an element of sinistral shear. The NW-striking rupture extended along the surface for approximately 21 km, with vertical surface offset observed to be 0.7 ± 0.1 m within a 500-1000 m deformation zone (Gold et al., 2019; King et al., 2021). Before field and interferometric data were obtained, it was speculated that the earthquake occurred along the Woodroffe Thrust, but following multiple field and geophysical studies, the consensus is that the likely source of the earthquake occurred on a previously unmapped back-thrust.

Prior to this work, only 75 aftershocks of local magnitude MLa 2.6 and greater had been detected by Geoscience Australia. However, only permanent ANSN stations were used in these initial aftershock locations, with the closest station located ~160 km away from the study area at Warrakurna, WA. This paper will present a significantly more comprehensive preliminary aftershock dataset following the 20 May 2016 mainshock by utilising the upgraded earthquake analysis capabilities within the NEAC. These preliminary aftershock locations will be used to support previously published observations and hypotheses on the tectonic controls of the 20 May 2016 Petermann Ranges earthquake. The development of this preliminary dataset will also serve as a starting point for a workflow to be applied to future aftershock

location analyses, which will provide valuable and more timely information on the rupture characteristics of intraplate earthquakes in Australia and their associated seismic hazard.

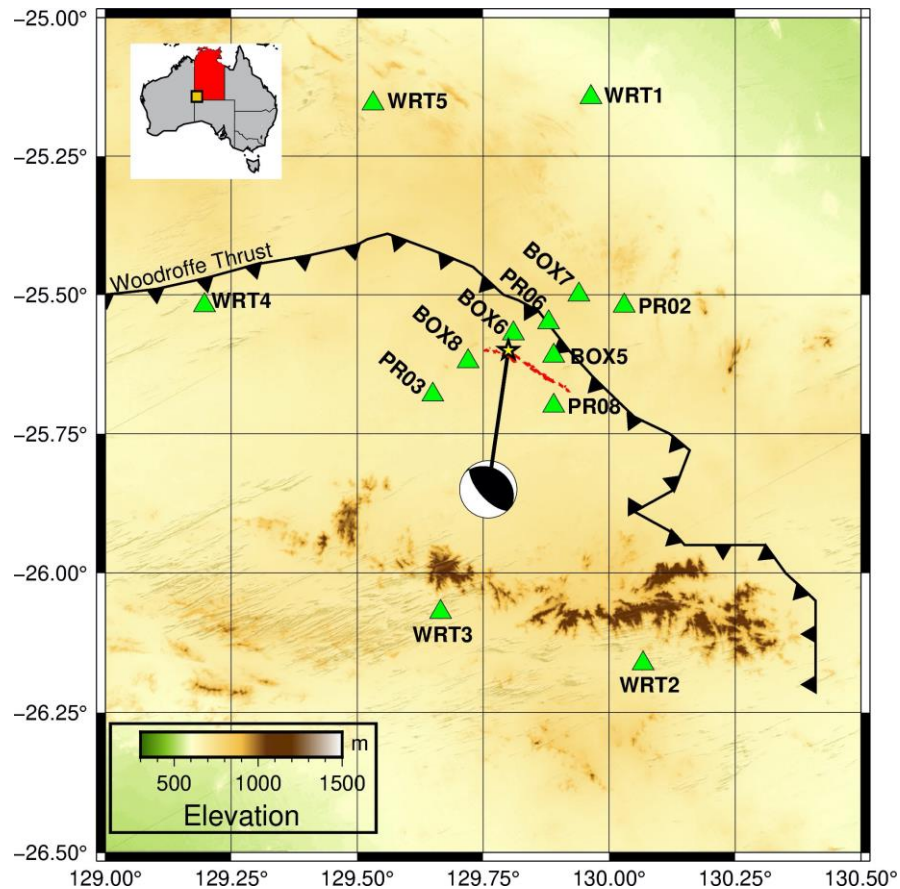


Figure 1. Station map of rapid deployment kits distributed around the epicentre of the 20 May 2016 Mw 6.1 mainshock. Study location is identified by the yellow box within the red outline of the NT in the top-left inset. The yellow star indicates the centroid location from Hejrani and Tkalčić (2019), and their centroid moment tensor (CMT) is represented as the black beachball. The ~21 km -long surface rupture is identified in red, and the approximate location of the Woodroffe Thrust is identified as the black thrust front.

2 Station Configuration

Thirteen aftershock kits were used in this analysis and were deployed by both Geoscience Australia and other academic institutions. Five stations (station codes BOX and PR) were deployed approximately perpendicular to the strike of the surface rupture, with three additional stations deployed in a staggered pattern to the east (Figure 1). These stations were deployed approximately six days following the mainshock and were decommissioned at the end of 2016. Five additional stations, WRT1 through WRT5, were deployed by the Australian National University more distal from the epicentre, in a pattern designed to maximise azimuthal coverage around the study area. The WRT stations were deployed from approximately 7 June to 17 September, 2016. Permanent Australian National Seismograph Network (ANSN) stations, i.e., AU.WRKA, were also incorporated in earthquake locations, but only the larger aftershocks typically above magnitude M_L 3.0 were visible at this station. Figure 2 shows the data availability for the BOX stations. From mid-June to mid-July, only one BOX station, BOX5,

was operational. Although not shown due to space limitations, stations PR04 to PR08 were online for only a very limited amount of time. Within this subset of PR stations, PR08 was the only continuously operating station but was only operational from early-June to end-July, 2016.

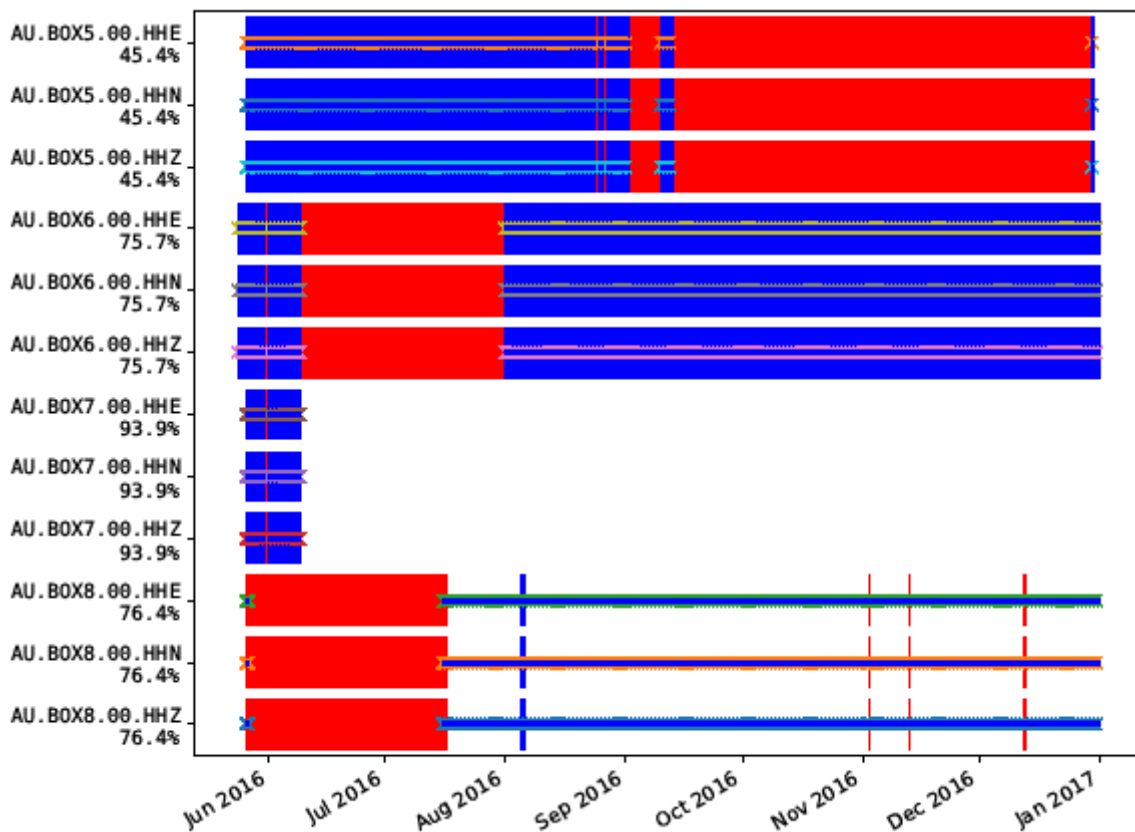


Figure 2. Data availability plot example for the four BOX* stations. The BOX* stations were deployed from approximately six days following the mainshock and decommissioned at the beginning of 2017. Gaps are indicated by both the red boxes and vertical red lines. Data overlap is indicated by the blue lines. BOX5 went offline in mid-September 2016, BOX6 went offline from mid-June to mid-July, and BOX8 was offline until mid-July. BOX7 was online for only 15 days.

3 SeisComP Methodology

Seismic data collected from all available stations were converted into a SeisComP Data Structure (SDS) archive, which allows for seamless playback of seismic waveform data that can be incorporated into SeisComP detection and event association modules (Weber et al., 2007). Automatic P- and S-wave picking was performed using the *scautopick* processing module, which applies a robust STA/LTA triggering algorithm to filtered waveform streams. Waveforms were initially filtered with a Butterworth highpass with a 15 Hz corner frequency to account for the high-frequency content of the smaller aftershocks. Then, a STA/LTA filter with a short-time window of 2 seconds and a long-time window of 80 seconds was applied. Once a pick is triggered, we utilise the *scanloc* algorithm to associate detected P-phases into a cluster, which is then used to form an event origin. The minimum number of P-phase picks for each cluster origin was set to a minimum threshold of four. Simultaneously, we apply the S-AIC S-phase picker, which allows for SeisComP to detect S-phases on the horizontal components once a P-phase is detected on a vertical component. This trigger utilises a 5 Hz high-pass filter which would activate 0.25 seconds after the detection of a P-phase. This short

time window accounts for the extremely short P-S travel time commonly observed on the closest station, BOX5.

All earthquakes were then located using the NonLinLoc locator algorithm (Lomax et al., 2000). A velocity model derived from the Tennant Creek, NT region (*tc1a*; Bowman et al., 1990) was chosen as the preferred velocity model, as no local velocity model for the Petermann Ranges has yet been created, and *tc1a* provides a better approximation of local crustal structure than the global-scale IASP91 velocity model. Each earthquake was manually analysed, and where visible, additional P- and S-phases were manually picked. A minimum of five phases were required to save the event into the database, with at least three P-phases and at least two S-phases.

4 Results

In total, 5278 earthquakes were automatically detected using the automated location methodology described above. Figure 3 shows a histogram that plots the number of earthquakes automatically detected for each day, beginning six days after the mainshock, and ending on 04 October 2016. From ~20 to 75 days following the 20 May mainshock, there exists a decrease in the number of detected earthquakes. This decrease in automatic detection of events is associated with poor station coverage, since for much of this period, only one BOX station, BOX5, was operational. This variability in station coverage unfortunately has led to catalogue incompleteness. Additionally, it has most recently been noticed that a parameter within the SeisComP *scautopick* module, “initTime”, which is required to define the automatic picking window, was set to 60 seconds. In other words, *scautopick* would reactivate only 60 seconds after a pick has been made. Thus, in cases when multiple events occurred immediately after each other and within 60 seconds, only one event was detected. With that said, a more comprehensive aftershock decay analysis will be reserved until the gaps and missed detections identified in this dataset have been addressed.

Over 80% of the detected earthquakes were recorded to have local magnitudes $MLa < 2.0$. Forty of the detected earthquakes were recorded to have local magnitudes $MLa \geq 3.0$. It is important to note that MLa magnitude equations still need to be tested at these short distances between the source and the stations.

The epicentral locations are presented in Figure 5. A majority of the earthquakes were located to the northeast of the surface rupture, extending towards the Woodroffe Thrust. The earthquakes are generally laterally constrained to the northwest and to the southeast along-strike of the ~21km fault rupture, forming a half-elliptical shape. At depth, the aftershock hypocentres are not well-constrained. Generally, aftershock hypocentres located closer to the surface rupture were shallower, with depths < 3 km, and decrease in depth along the A-A' transect. Most aftershocks to the northeast of the surface rupture were constrained to depths < 5 km. Furthermore, there exists a large cluster of earthquakes located to the southwest of the mapped surface rupture.

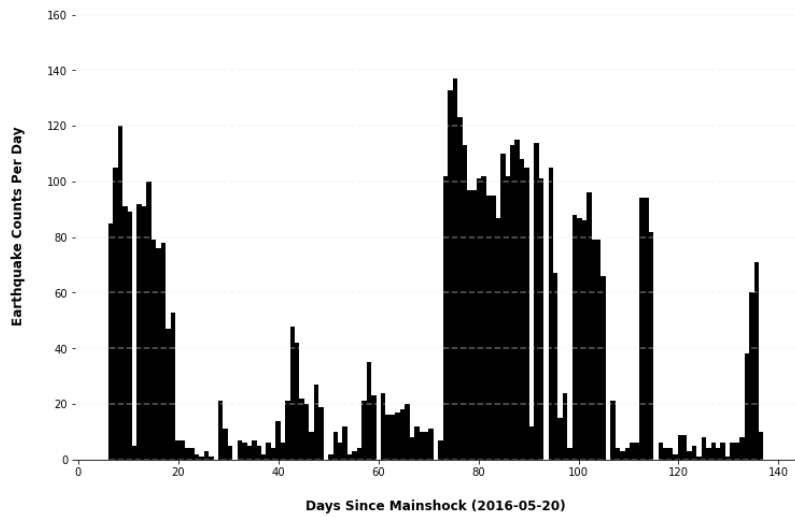


Figure 3. Aftershock automatic detection count per day following the 20 May 2016 mainshock. Days since the mainshock are plotted along the x-axis with daily detections plotted on the y-axis. The drop in automatic detections from Day 20 to Day ~75 is most likely attributed to the lack of available stations online during this time period. When at least three stations were online at a given time, over 100 event detections were made.

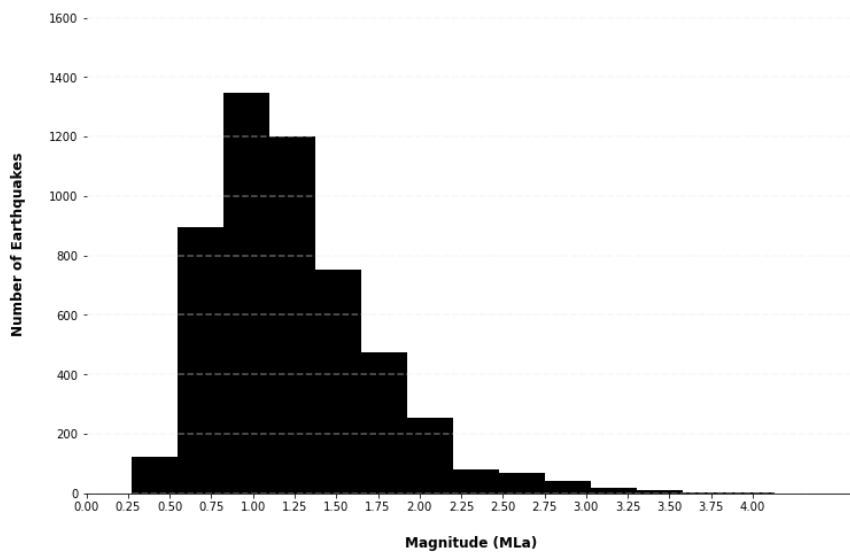


Figure 4. Magnitude versus frequency plot, displaying the distribution of detected magnitudes within this dataset.

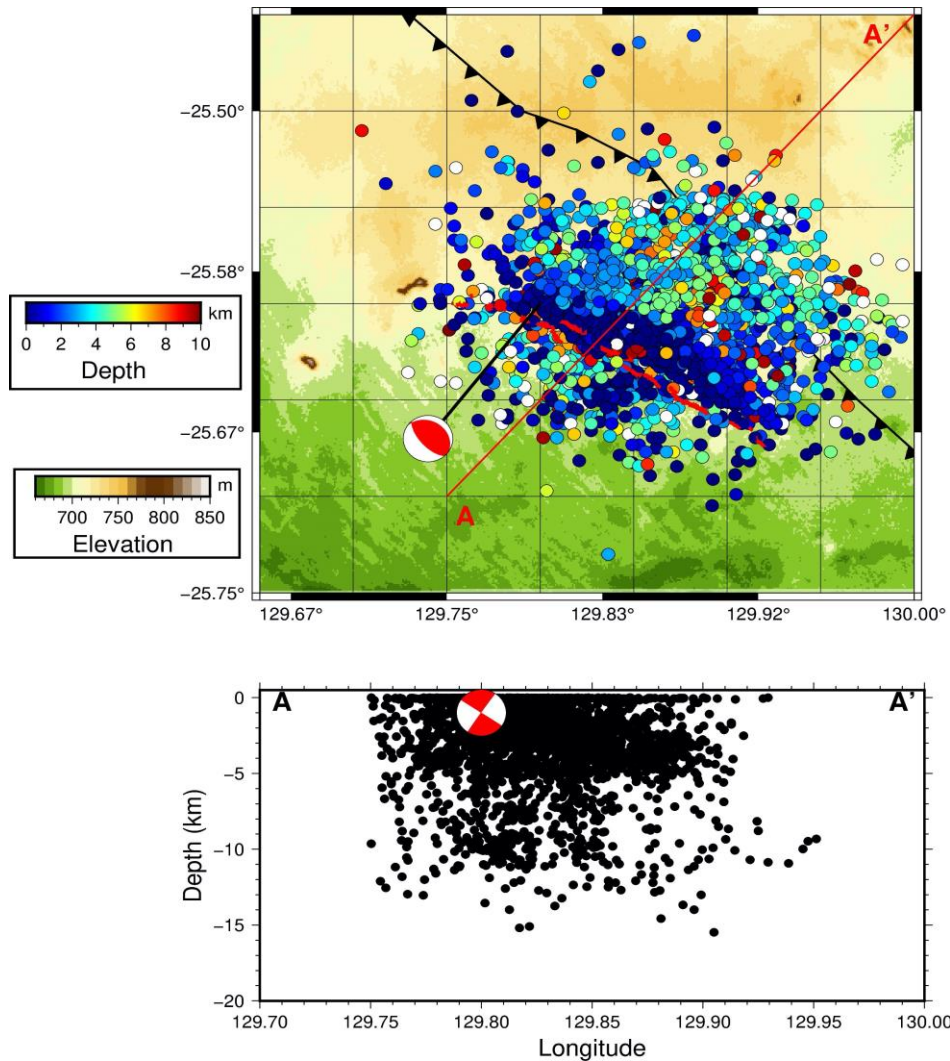


Figure 5. Aftershock location map. (a) Epicentres are displayed as circles, with their colour corresponding with depth. Surface rupture is shown in red. Hejrani and Tkalčić (2019) moment tensor solution is plot as the red focal mechanism. The Woodroffe Thrust is displayed as the black fault front. (b) Earthquake hypocentres projected onto the A-A' transect.

5 Discussion and Future Work

The preliminary spatial distribution of aftershocks following the 20 May 2016 Petermann Ranges earthquake correlate with the deformation geometries revealed by optical satellite imagery and digital elevation models (DEMs) presented by Gold et al. (2019), who also reveal a half-elliptical form in the hanging wall of the ruptured fault. This aftershock distribution similarly supports the co-seismic deformation modelling results by Wang et al. (2019) and Polcari et al. (2018), who provide evidence of dominant deformation in the hanging wall, little deformation in the footwall, with deformation in the footwall similarly following a half-elliptical shape along-strike of the arcuate surface rupture.

This aftershock catalogue similarly correlates with the centroid moment tensor (CMT) inversion presented by Hejrani and Tkalčić (2019), who constrain the mainshock at 1 km depth, with an estimated moment magnitude M_w 5.9 suggesting a ~4 km down-dip rupture. The depth of hypocentres of this catalogue also support the co-seismic slip model presented by Wang et al. (2019), who suggest a maximum slip that is concentrated at shallow depths, between 0 and 3 km.

While this aftershock catalogue strongly supports broad hanging wall deformation along a backthrust of the Woodroffe Thrust, additional relocation analyses is required to better constrain the aftershocks along a defined rupture plane. Relocation analysis will also be required to determine if aftershocks could have been triggered along the Woodroffe Thrust and within the footwall of the causative fault. Lastly, the SeisComP software package will be an invaluable resource for earthquake monitoring within the NEAC for many years to come. By utilizing the tools within this package, an operational workflow will be designed to build on the above methodology, which will allow seismologists at Geoscience Australia to more rapidly locate aftershocks following significant events. The most recent 22 September 2021, M_w 5.9 Woods Point, Victoria earthquake will be an ideal case study to test this methodology when the data from the aftershock deployment become available. Overall, by having an up-to-date Australian earthquake catalogue that includes complete aftershock datasets, Geoscience Australia can more efficiently deliver accurate earthquake products that will be of great benefit to both the Australian public and seismological research community.

6 Conclusions

This paper presents the most comprehensive aftershock catalogue following the 20 May 2016 M_w 6.1 Petermann Ranges earthquake, supporting the previously published observations that the causative fault for this event was a previously unidentified back thrust of the Woodroffe Thrust and not the Woodroffe Thrust itself. The epicentral distribution of aftershocks form a half-elliptical shape within the back-scarp zone, extending to the northeast of the mapped linear surface rupture and corresponding geometrically with the distribution of deformation as identified by both DEM and InSAR observations (Clark et al., 2020).

Additionally, by utilising the advanced automatic location capabilities available within the SeisComP software that is now operational within the NEAC at Geoscience Australia, it will be possible to replicate similar location procedures for future temporary seismic deployments following significant intraplate earthquakes. These capabilities will allow for timelier aftershock analyses that can be efficiently combined with field and geodetic observations, which can lead to a more comprehensive understanding of intraplate faulting within the stable continent of Australia. Additional work is required to better constrain the focal depths of these aftershocks, which will help to better identify and delineate the shallow faults in this part of Australia.

7 References

- Allen, T.I. (2019). Seismic hazard estimation in stable continental regions: Challenges and opportunities, In: Proceedings of the 2019 Pacific Conference on Earthquake Engineering, Paper No. 0392. Auckland, New Zealand, 4–6 April.
- Bowman, J. R., G. Gibson, and T. Jones (1990). Aftershocks of the 1988 January 22 Tennant Creek, Australia intraplate earthquakes: evidence for a complex thrust-fault geometry, *Geophys. J. Int.* **100**, 87-97, doi: 10.1111/j.1365-246X.1990.tb04570.x.
- Clark, D, McPherson, A., and Dissen, R.V. (2012). Long-term behavior of Australian stable continental region (SCR) faults, *Tectonophysics*, Vol. 566-567, pp. 1-30, doi: <https://doi.org/10.1015/j.tcto.2012.07.004>.
- Clark, D. J., S. Brennand, G. Brenn, M. C. Garthwaite, J. Dimech, T. I. Allen, and S. Standen (2020). Surface deformation relating to the 2018 Lake Muir earthquake sequence, southwest Western Australia: new insight into stable continental region earthquakes, *Solid Earth* **11**, 691–717, doi: 10.5194/se-11-691-2020.
- Gold, R. D., Clark, D., Barnhart, W. D., King, T., Quigley, M., and Briggs, R. W. (2019). Surface rupture and distributed deformation revealed by optical satellite imagery: The intraplate 2016 Mw 6.0 Petermann Ranges earthquake, Australia, *Geophysical Research Letters*, Vol. 46, doi: 10.1029/2019GL084926.
- Hejrani, B. and Tkalčić H. (2019). The 20 May 2016 Petermann Ranges earthquake: centroid location, magnitude and focal mechanism from full waveform modelling, *Australian Journal of Earth Sciences*, Vol 66, No 1, pp 37-45, doi: 10.1080/08120099.2018.1525783.
- Johnston, A. C. (1994b). The stable continental region earthquake database, in *The Earthquakes of Stable Continental Regions, Assessment of Large Earthquake Potential* Johnston, A. C., K. J. Coppersmith, L. R. Kanter, and C. A. Cornell (Editors), Vol. 1, Electric Power Research Institute, Pleasant Hill, CA, Chap. 3, 3-1–3-75.
- Jones, T. D., G. Gibson, K. F. McCue, D. Denham, P. J. Gregson, and J. R. Bowman (1991). Three large intraplate earthquakes near Tennant Creek, Northern Territory, on 22 January 1988, *BMR J. Aust. Geol. Geophys.* **12**, 339-343.
- Lomax, A., J. Virieux, P. Volant, and Berge-Thierry, C. (2000). Probabilistic earthquake location in 3D and layered models, in *Advances in Seismic Event Location*, Springer, Dordrecht, The Netherlands, pp. 101–134.
- King, T. R., M. Quigley, D. Clark, A. Zondervan, J. H. May, and A. Alimanovic (2021). Paleoseismology of the 2016 M_w 6.1 Petermann earthquake source: implications for intraplate earthquake behaviour and the geomorphic longevity of bedrock fault scarps in a low strain-rate cratonic region, *Earth Surf. Processes Landforms* **46**, 1238-1256, doi: 10.1002/esp.5090.
- Polcari M, Albano M, Atzori S, Bignami C, and Stramondo S. (2018). The Causative Fault of the 2016 Mw 6.1 Petermann Ranges Intraplate Earthquake (Central Australia) Retrieved by C- and L-Band InSAR Data. *Remote Sensing*, Vol 10, No 8, p. 1311, doi: <https://doi.org/10.3390/rs10081311>.
- Shelly, D.R. (2020). A High-Resolution Seismic Catalog for the Initial 2019 Ridgecrest Earthquake Sequence: Foreshocks, Aftershocks, and Faulting Complexity. *Seismological Research Letters*, Vol. 91, No. 4, pp. 1971–1978, doi: <https://doi.org/10.1785/0220190309>.

- Waldhauser, F., and Ellsworth, W.L. (2000). A double-difference earthquake location algorithm: method and application to the northern Hayward fault, California. *Bulletin of the Seismological Society of America*, Vol. 90, No. 6, pp. 1353-1368, doi: <https://doi.org/10.1785/0120000006>.
- Weber, B., J. Becker, W. Hanka, A. Heinloo, M. Hoffmann, T. Kraft, D. Pahlke, J. Reinhardt, J. Saul, and H. Thoms (2007). SeisComP3 - automatic and interactive real time data processing, *Geophys. Res. Abs.* **9**, 09219, SRef-ID: 1607-7962/gra/EGU2007-A-09219.